OPEN ACCESS

Dynamic MAPK/ERK Activity Sustains Nephron Progenitors through Niche Regulation and Primes Precursors for Differentiation

Anneliis Ihermann-Hella,[1] Tsuyoshi Hirashima,[2] Jussi Kupari,[1,8] Kristen Kurtzeborn,[1] Hao Li,[1] Hyuk Nam Kwon,[1] Cristina Cebrian,[3] Abdul Soofi,[4] Arvydas Dapkunas,[5] Ilkka Miinalainen,[6] Gregory R. Dressler,[4] Michiyuki Matsuda,[2] and Satu Kuure[1,7,*]

[1]HiLIFE and Medicum, University of Helsinki, Helsinki FIN-00014, Finland
[2]Department of Pathology and Biology of Diseases, Graduate School of Medicine & Laboratory of Bioimaging and Cell Signaling, Graduate School of Biostudies, Kyoto University, Kyoto 606-8501, Japan
[3]Developmental Biology Division, Cincinnati Children's Hospital, Cincinnati, OH 45229, USA
[4]Department of Pathology, University of Michigan, Ann Arbor, MI 48109, USA
[5]Medicum and Meilahti Clinical Proteomics Core Facility/HiLIFE, University of Helsinki, Helsinki FIN-00014, Finland
[6]Department of Pathology (Biocenter Oulu), University of Oulu, Oulu 90220, Finland
[7]GM-Unit, LAC/ HiLIFE, and Medicum, University of Helsinki, Helsinki FIN-00014, Finland
[8]Present address: Division of Molecular Neurobiology, Department of Medical Biochemistry and Biophysics, Karolinska Institutet, SE-17177, Sweden
*Correspondence: satu.kuure@helsinki.fi
https://doi.org/10.1016/j.stemcr.2018.08.012

SUMMARY

The *in vivo* niche and basic cellular properties of nephron progenitors are poorly described. Here we studied the cellular organization and function of the MAPK/ERK pathway in nephron progenitors. Live-imaging of ERK activity by a Förster resonance energy transfer biosensor revealed a dynamic activation pattern in progenitors, whereas differentiating precursors exhibited sustained activity. Genetic experiments demonstrate that MAPK/ERK activity controls the thickness, coherence, and integrity of the nephron progenitor niche. Molecularly, MAPK/ERK activity regulates niche organization and communication with extracellular matrix through PAX2 and ITGA8, and is needed for CITED1 expression denoting undifferentiated status. MAPK/ERK activation in nephron precursors propels differentiation by priming cells for distal and proximal fates induced by the Wnt and Notch pathways. Thus, our results demonstrate a mechanism through which MAPK/ERK activity controls both progenitor maintenance and differentiation by regulating a distinct set of targets, which maintain the biomechanical milieu of tissue-residing progenitors and prime precursors for nephrogenesis.

INTRODUCTION

The mitogen-activated protein kinase/extracellular signal-regulated kinase (MAPK/ERK, henceforth referred to "MAPK") pathway is a protein-serine/threonine kinase cascade consisting of Ras, Raf, and dual-specificity mitogen-activated protein kinases (MEK1/2) that fully activate the effector kinases ERK1/2 (Roskoski, 2012). MAPK activation is best defined in response to growth factor stimulation of receptor tyrosine kinases (RTKs) and downstream of integrin signaling (McKay and Morrison, 2007). Mapping of MAPK activity in early post-implantation embryos has revealed discrete domains of both sustained and dynamic activities (Corson et al., 2003). The molecular level variation in magnitude and duration of the activation produces distinct cellular responses (Chambard et al., 2007; Pouyssegur et al., 2002). The importance of MAPK activity in morphogenesis is emerging (Boucherat et al., 2015; Parada et al., 2015; Scholl et al., 2007), but its function in the maintenance and fate determination of tissue-specific progenitors remains to be determined.

The developing kidney holds progenitor populations that undergo differentiation and complex morphogenesis to yield a functional organ. The nephron progenitors (NPs), capable of giving rise to all segments of functional nephrons, are of great interest because of their potential as a source for novel treatment strategies for kidney diseases (Little, 2016). They surround each ureteric bud (UB) tip while themselves being enclosed by stromal progenitors. Such tissue organization establishes a progenitor niche where inductive interactions through intercellular and population-intrinsic communications regulate progenitor actions (O'Brien and McMahon, 2014). Of these, fibroblast growth factor (FGF) signaling through FGF receptors (FGFR) 1 and 2 is indispensable for lineage specification, expansion, and viability of NP cells (Poladia et al., 2006). NP survival is enhanced by several FGF ligands, although targeted disruption identified FGF9 and 20 as the most crucial regulators of progenitor maintenance, self-renewal, and stemness (Barak et al., 2012; Brown et al., 2011). *Fgf8* is expressed at the onset of nephrogenesis and is essential for nephron cell survival and distal differentiation (Grieshammer et al., 2005; Perantoni et al., 2005). Importantly, the population-intrinsic intracellular cascades evoked downstream of FGFRs in NPs remain to be studied, despite suggested functions in *ex vivo* kidney cultures (Lindstrom et al., 2015).

NPs form a heterogeneous mixture of progenitors whose purpose for divergence remains obscure (Boyle et al., 2007; Park et al., 2012; Self et al., 2006; Short et al., 2014). In this study, we utilized live-imaging to reveal dynamic and
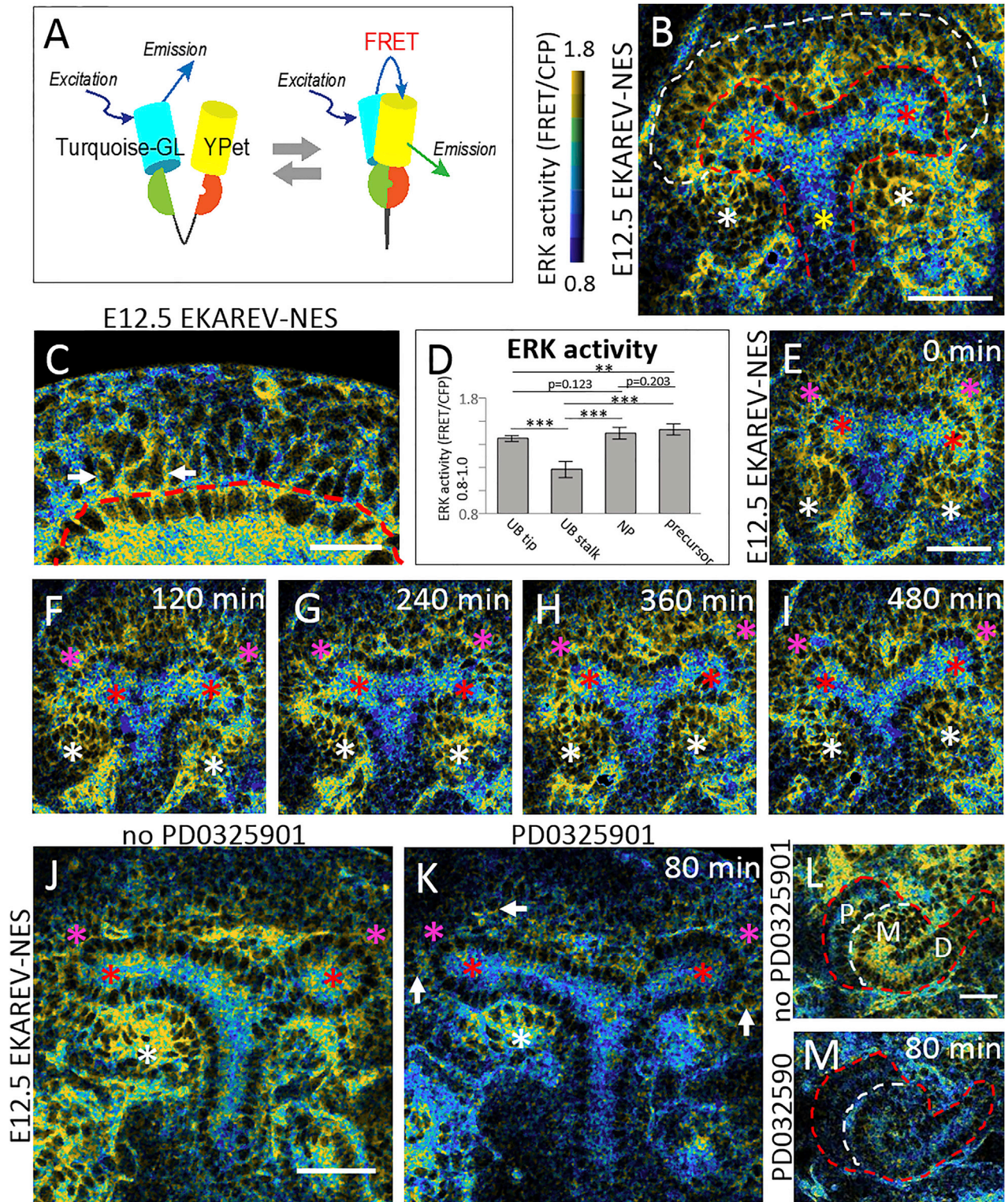
Figure 1. NPs Sustain High Levels of MAPK/ERK Activity

(A) Schematic of the intramolecular Förster resonance energy transfer (FRET)-based biosensor for ERK activity.

(B) ERK activity map of EKAREV-NES transgenic E12.5 kidney. Color represents ERK activity quantified by the ratio of FRET to cyan fluorescent protein intensity. A red dotted line designates the ureteric bud (UB), and a white dotted line outlines NPs. Red

(legend continued on next page)

heterogeneous MAPK activation in NPs of embryonic kidneys and more persistent activity in the distal domains of renal vesicles (RVs). Such patterns suggest that MAPK activity may play an essential role in NP population maintenance and differentiation. By conditional inactivation of MAPK activity in NPs, we demonstrate that loss of MAPK activity does not fully phenocopy the renal pathology of FGF mutants, and thus may provide new insights into the genetics of congenital kidney defects.

RESULTS

ERK Biosensor Reveals Dynamic MAPK/ERK Activation in NPs

We previously observed that pERK1/2 staining, used as a readout of MAPK activity, localizes to several progenitor cell populations of the developing kidney (Ihermann-Hella et al., 2014). To reveal the magnitude as well as temporal and spatial distribution of MAPK activation, live-imaging of transgenic mice expressing a Förster resonance energy transfer (FRET)-based biosensor of ERK activity was used (Komatsu et al., 2011) (Figure 1A). FRET analysis revealed that ERK activity exhibits a heterogeneous pattern in embryonic day 12.5 (E12.5) kidneys (Figure 1B). The highest levels of ERK activity localized to UB tip cells, NPs and differentiating nephron precursors. ERK activity levels varied between adjacent NP cells, including those of the first layer, which are in direct contact with the UB (Figure 1C). Sub-tissue scale ERK activity measurements revealed similar magnitudes in NPs and UB tip cells (Figure 1D), and the precursors showed slightly higher activity (p < 0.01). Time-lapse analysis of cultured kidneys revealed that ERK activity remains high during NP differentiation and subsequent nephrogenesis (Figures 1E–1I). Overall, MAPK activity was retained in NPs, precursors, and UB tips, while the proximal segments of differentiating S-shaped bodies (SSBs) exhibited lower activity (Figures 1E–1I and 1L; Video S1).

To discern the dynamic range of the ERK biosensor, the transgenic kidneys were treated with 50 ng/mL FGF2 to observe a marked upregulation of the FRET signal in the UB, NPs, and, to a lesser extent, in RVs (Figures S1A–S1C; Video S2). Further validation revealed that MEK inhibition (100 nM PD0325901) caused an almost complete loss of ERK activity in the UB tips and SSBs already after 80 min (Figures 1J–1M). A more heterogeneous downregulation was seen in the mesenchyme, where a subset of NP cells retained ERK activity markedly longer than their neighboring cells (Figures 1J and 1K; Video S3). Similarly, RVs sustained ample ERK activation throughout the 590-min imaging period. These data indicate that two possible ERK activation mechanisms occur in the developing kidney; a rapid and transient activation where a continuous upstream MEK activity is needed for ERK phosphorylation in the majority of NPs, in UBs, and in SSBs, while a subset of NP cells and RVs sustain ERK phosphorylation irrespective of MEK inhibition.

MAPK/ERK Activity Is Required for the Expression of a Subset of NP Regulators

To study the functional requirement of MAPK activity *in vivo*, we deleted *Mek1* specifically from NPs with *Six2-Tet-off-eGFPCre* (*Six2-TGC$^{tg/+}$*) (Kobayashi et al., 2008). As described, some *Six2$^+$* cells fail to express CRE recombinase and associated GFP (Kobayashi et al., 2008), but when crossed to *Mek1* floxed mice (*Mek1$^{F/F}$*), MEK1 protein was lost in the majority of NPs and nephron precursors at E13.5 (Figures S1D–S1F'). Breeding with *Mek2* conventional knockout (*Mek2$^{−/−}$*) depleted MAPK activity from *Six2-TGC$^{tg/+}$;Mek1$^{F/F}$;Mek2$^{−/−}$* (henceforth referred as double-knockout "dko") NPs and the descendant RV cells but not in three control genotypes (*Mek2$^{+/−}$*, *Mek2$^{−/−}$*, and *Six2-TGC$^{tg/+}$;Mek1$^{F/+}$;Mek2$^{+/−}$*; Figures S1G and S1H).

NP viability, self-renewal, and maintenance of progenitor identity depend on SIX2, Wilms tumor protein homolog 1 (WT1), PAX2, and CITED1 (Boyle et al., 2007; Donovan et al., 1999; Naiman et al., 2017; Park et al., 2012).

asterisks mark UB tips and yellow asterisk shows the UB stalk. White asterisks indicate differentiating nephron precursors. Scale bar, 50 μm.

(C) Higher magnification of the NPs. Arrows indicate individual NPs with high ERK activity. A red dotted line designates the UB. Scale bar, 30 μm.

(D) Quantification of ERK activity in the indicated cell populations (n = 3 independent kidneys, each indicated cell population sampled nine times). **p < 0.01; ***p < 0.001.

(E–I) Time-lapse snapshots of ERK activity map of transgenic E12.5 kidney from 0 to 480 min. Red asterisks mark UB tips, pink asterisks show NPs, and white asterisks indicate differentiating nephron precursors. Scale bar, 50 μm.

(J and K) ERK activity map of transgenic E12.5 kidney without and with MEK inhibitor treatment (80 min after addition of 100 nM PD0325901). Red asterisks mark UB tips, pink asterisks show NPs, and white asterisks marks a nephron precursor. Arrows indicate NPs where high ERK activity is sustained regardless of inhibition in (K). Scale bar, 50 μm.

(L and M) Higher magnification of an S-shaped body without and with MEK inhibitor treatment. A red dotted line outlines the S-shaped body, and a white dotted line separates distal (D) and medial (M) domains from the proximal (P) domain. Scale bar, 30 μm.

See also Figure S1.
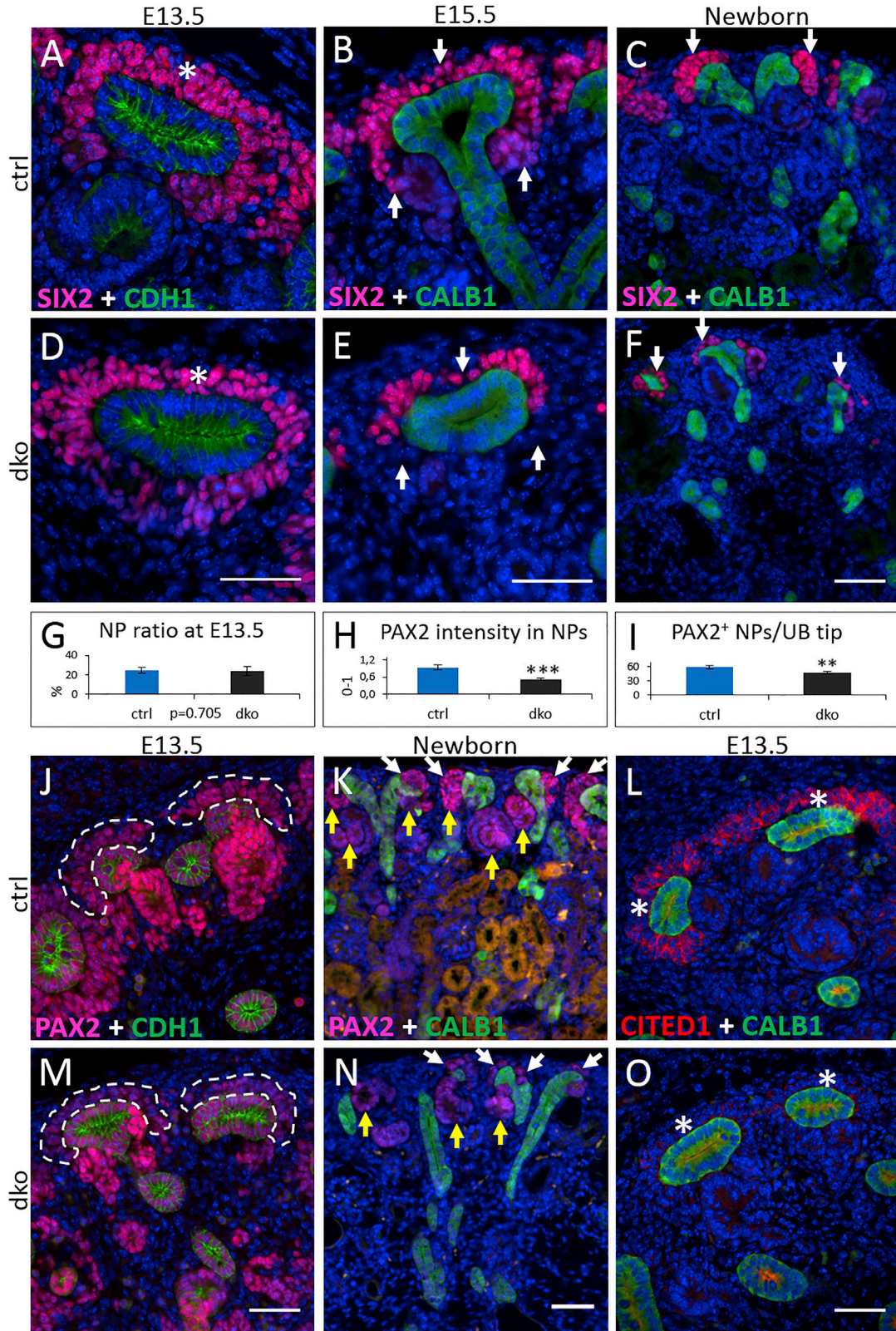
SIX2[+] NPs surround the UB tips as an undifferentiated NP pool throughout renal morphogenesis until post-natal day 3 (P3) (Hartman et al., 2007) (Figures 2A–2C). Initially, SIX2^{+} NPs surrounded UB tips in equal proportion in dko and control kidneys, but a progressive decrease in the quantity of NPs occurred from mid-gestation onward (Figures 2A–2G). Despite the gradual decrease in number, the remaining dko NPs retained normal levels of SIX2 and WT1 (Figures 2A–2F, S2A, and S2B).

Examination of PAX2 revealed a 44% reduction in the E13.5 dko NP population, indicating a marked reduction in protein levels (Figures 2H, 2J, and 2M; p < 0.001). Additional quantification of PAX2^{+} NP quantity showed a significant 19% reduction in the dko kidneys (Figure 2I; p < 0.01), implying that a subset of NPs had lost PAX2 altogether as the total number of SIX2^{+} cells remained unchanged (Figure 2G). The decrease in PAX2 level and NP amount persisted in the dko until birth, unlike in the control kidney where ample NP populations were maintained (Figures 2C, 2F, 2K, and 2N). To verify the regulatory relation between MAPK activation and PAX2, we chemically inhibited MEK in mouse kidney 4 (mK4) cell line and found that reduced MAPK activity negatively impacts PAX2 levels (Figure S2C). Lastly, we discovered that immunoreactivity to CITED1, a protein proposed to demarcate the uninduced NP population among all NP cells (Brown et al., 2013), was severely diminished in dko NPs at E13.5 (Figures 2L and 2O). In summary, our data show that MAPK activity is required not only for the maintenance of the NP population but also for their specific features potentially regulated by PAX2 and CITED1 activities.

NP Self-Renewal Depends on MAPK/ERK Activity

In various cell types, MAPK activity promotes proliferation, especially by driving G1 and G2/M phase progression (Chambard et al., 2007). Persistent proliferation in the NP compartment maintains the NP population throughout embryonic and early post-natal stages and replenishes induced NPs (Short et al., 2014). Visualization of replicating NPs after a 1-hr pulse of 5-ethynyl-2′-deoxyuridine (EdU) and a DNA content-based cell-cycle analysis performed to sorted NPs revealed a 20% decrease in cycling

dko NPs and a 22% drop in dko NPs in S phase (Figures 3A–3E; p < 0.05). Consequently, dko NPs progressing through G2/M phases were reduced by 35% (p < 0.05) without significant differences in G1 populations. The data indicate that continuous MEK activity is required for ERK phosphorylation in the majority of NPs, in SSBs, and in the UB epithelium, which are all actively proliferating tissues (Figures 1J–1M and 3A). Thus, dynamic ERK activation appears to relate to proliferation as a specific cellular function in the developing kidney. In conclusion, the MAPK pathway promotes NP cell-cycle progression, thus enabling sufficient NP maintenance throughout development.

Since the amount of dko progenitors declines rapidly as development proceeds, we explored whether MAPK would additionally affect NP viability. As shown before, apoptosis is a rare event among NPs (Hartman et al., 2007), and no differences were detected between the control and dko NPs at E13.5 (Figures S2D and S2E). Yet, a minor increase in the cleaved caspase-3[+] dko NPs was detected at E15.5 (Figures S2F and S2G), suggesting that increased cell death at later stages may contribute to the phenotype worsening.

Progenitor Organization within the Niche Requires MAPK/ERK Activity

NP population is maintained at a specific tissue niche, which is a cohesive structure of five cell layers where the first layer interacts with the UB epithelium, and the outermost NPs are in contact with the stromal cell population (O'Brien and McMahon, 2014). NPs exhibit columnar alignment toward the UB and adhere more tightly to each other than to the surrounding stromal cells (Uchiyama et al., 2010). Although the amount of layers and NPs decreases over time (Short et al., 2014), the NP organization remains similar, especially at the first layer in contact with the UB. We next analyzed cell profiles in the first layer of NPs immediately adjacent to the UB epithelium. In E13.5 control kidneys, three layers of NP cells were detected, and the NP perimeter, as revealed by cell surface labeling of catenin δ-1 (CTNND1), was on average 42 μm and roundness was 0.4 out of 1 (Figures 3F, 3H,

---

Figure 2. MAPK/ERK-Deficient NPs Are Misregulated and Exhausted during Development

(A–F) Control (ctrl) and dko embryonic kidneys immunostained for SIX2 (NPs) and CDH1, CALB1 (ureteric bud [UB] epithelium). Asterisks mark NPs in (A) and (D). Arrows indicate NPs in (B), (C), (E), and (F). Scale bars, 50 μm.

(G) Quantification of GFP[+] NPs from flow cytometry analysis of E13.5 whole kidney lysates (ctrl n = 34, dko n = 22 independent samples).

(H) NP population to UB intensity ratio of PAX2 immunostaining in E13.5 kidneys. ***p < 0.001.

(I) Quantification of PAX2^{+} NPs per UB tip in E13.5 kidneys. **p < 0.01.

For (H and I), n = 3 independent kidneys, each containing nine measurements.

(J–O) Ctrl and dko embryonic kidneys immunostained for PAX2 (NPs, nephron precursors, and UB epithelium), CITED1 (NPs), and CDH1, CALB1. Dotted lines outline the PAX2^{+} NPs in (J) and (M). White arrows indicate NPs and yellow arrows show nephron precursors in (K) and (N). Asterisks indicate NPs in (L) and (O). Scale bars, 50 μm.
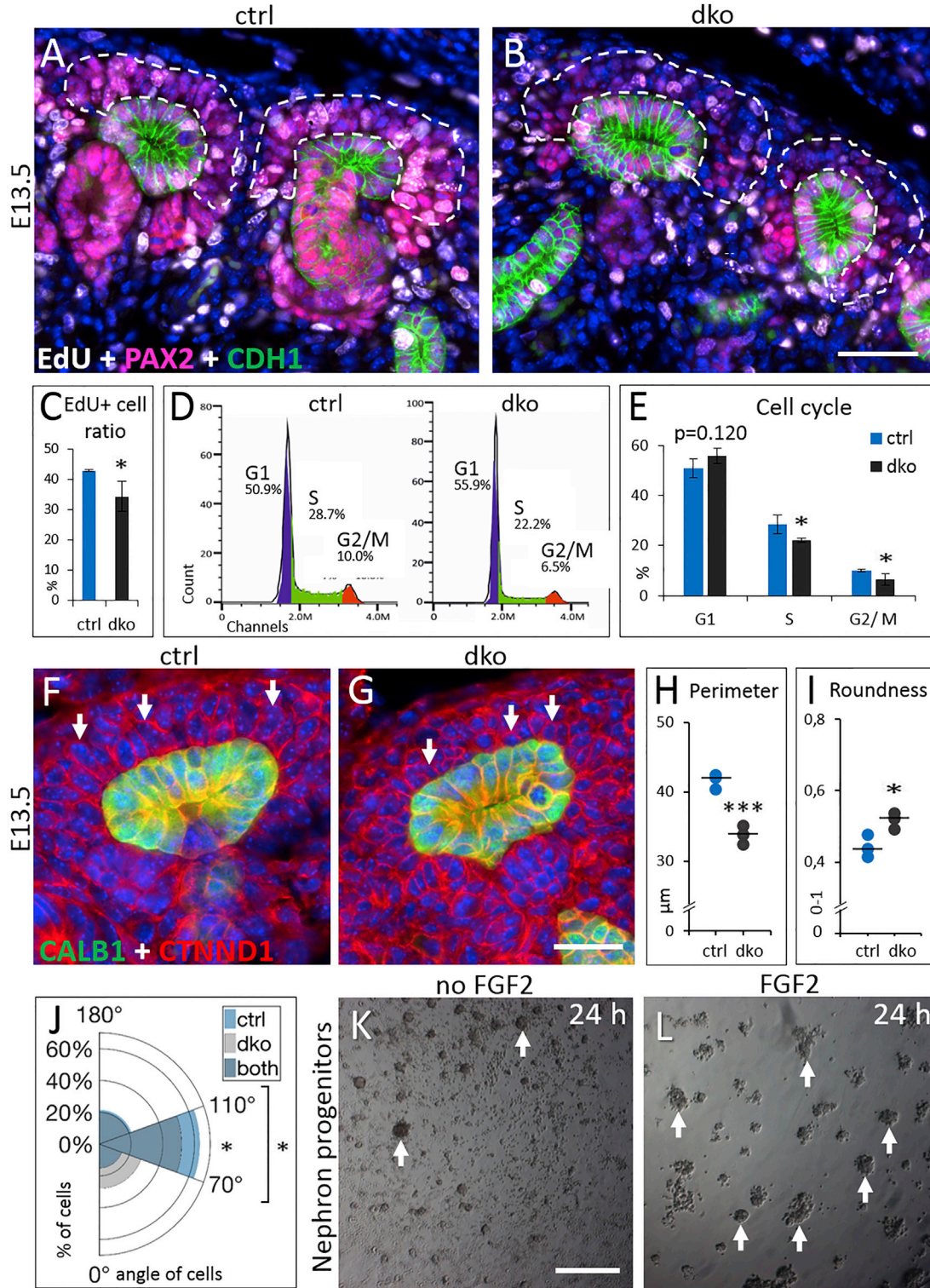
See also Figures S1 and S2.

Figure 3. MAPK/ERK Activity Promotes NP Self-Renewal and Maintains Niche Organization

(A and B) Control (ctrl) and dko E13.5 kidneys immunostained for PAX2 (NPs, nephron precursors, and UB epithelium), CDH1 (nephron precursors and UB epithelium), and EdU-labeled (replicating cells). Dotted lines outline the PAX2/EdU⁺ NPs. Scale bar, 50 μm.

(C) Quantification of EdU⁺ cell ratio from PAX2⁺ NPs (n = 3 independent kidneys, each containing nine measurements). *p < 0.05.

(legend continued on next page)

and 3I). Measurements of the cell's attachment angle to the epithelium showed that 64% of NPs oriented between 70° and 110° toward the epithelium, with the remaining 36% of NPs being more tilted, at an angle under 70° or over 110° (Figure 3J). Analysis of potential differences in NP properties arising from the NP localization (medial or lateral around the UB tip) revealed a uniform range regardless of localization (Figure S3A). Based on the independent variation among variables (Figure S3B), the NP properties are likely regulated through various cellular mechanisms. Our characterization shows that the control NPs interacting with the UB are relatively small but elongated cells, situated perpendicular toward the UB epithelium.

Characterization of the NP niche in dko kidneys revealed an apparent cellular disorganization and variation in its thickness, coherence, and integrity (Figures 3F, 3G, S3C, and S3D′). Analysis of dko cell profile and orientation toward the UB showed a 19% drop in cell perimeter, while cell roundness had increased by 15% (Figures 3H and 3I; $p < 0.001$/$p < 0.05$, respectively). Furthermore, 17% less dko NPs were oriented between 70° and 110°, while 23% of the dko NPs exhibited a more tilted orientation (Figure 3J; $p < 0.05$). The contact surface length between the NP and UB in dko remained unchanged (Figure S3E). We hypothesized that if the cell size of NPs is an intrinsically regulated property, flow cytometry analysis should present dko NPs as smaller sized cells. Instead, if interactions with the niche affect cell size, the smaller perimeter in an intact environment (whole kidney) would not be detected by flow cytometry. Analysis of NP cells failed to reveal differences in cell size between GFP$^+$ control and dko NP populations (30 control/24 dko kidneys; $p = 0.179$), as an average of 44.8% (SD = 9.98) of control and 49.7% (SD = 8.13) of dko cells fell into a small cell category.

Visualization of the cortical stroma revealed rare intermingling stromal cells among the NPs, but no clear differences between the control and the dko were detected (Figures S3F and S3G), suggesting that increased stromal intrusion does not contribute to the phenotype. These data demonstrate that MAPK activity regulates fundamental cellular properties of the NPs and contributes to the maintenance of a highly coherent NP niche architecture.

PAX2 and ITGA8 Mediate MAPK/ERK-Dependent Niche Orientation and Interactions

Since cellular adhesion is critical for establishing tissue architecture (Narva et al., 2017), we analyzed expression of typical NP adhesion proteins. CTNND1, neural cell adhesion molecule 1, cadherin 2 (CDH2), and catenin β-1 staining and electron microscopy of adhesive sites in dko NPs were comparable with control NPs (Figures 3F, 3G, S3C, S3D′, and S4A–S4J). Functional tests of NP adhesive properties in a sphere-forming assay revealed that FGF2 treatment promoted NP cell survival and faster aggregation into larger and more abundant spheres (Figures 3K and 3L; Video S4).

Integrin α8 (ITGA8) mediates NP interaction with the surrounding environment, especially with the UB. It appears to control NP cells' basolateral integrity and their condensation (Muller et al., 1997; Uchiyama et al., 2010). ITGA8 showed a strong basal localization in the first layer of control NP cells and additional lower level lateral localization (Figures 4A and 4B′). Interestingly, ITGA8 showed more intense basal localization in E13.5 dko NPs, while focal and reduced intensity was seen in lateral membranes (Figures 4C and 4C′). In contrast, E15.5 dko NPs had a nearly complete loss of ITGA8, which coincided with the NP cohesion defect worsening (Figures 4D and 4D′).

MAPK activity's effect on ITGA8 was further verified by flow cytometry of NPs in control and MEK-inhibited (15 μM UO126) kidneys, where cell surface expression of ITGA8 was analyzed in live cells. This revealed a statistically significant decrease in ITGA8 on the cell surface of MAPK-deficient NPs ($p < 0.01$) and a 13% decline in the positively stained cell population (Figures 4E and 4F; $p < 0.001$). On the contrary, MEK inhibition in embryonic lung, which shows high endogenous MAPK activation and ITGA8 expression, but has different molecular milieu than NPs (Boucherat et al., 2015), showed no changes in ITGA8 (Figures S4K and S4L). The localization of ITGA8 ligand nephronectin and ECM proteins fibronectin and laminin-111 were also unchanged in the dko kidneys (Figures S5A–S5J′).

(D and E) DNA content-based cell-cycle analysis performed on sorted E13.5/E14.5 GFP$^+$ NPs (ctrl n = 4 and dko n = 3 independent samples, each containing 10,000 cells pooled from collected kidneys). *$p < 0.05$.

(F and G) Ctrl and dko E13.5 kidneys immunostained for CTNND1 (NP, UB epithelium, and stroma) and CALB1 (UB epithelium). Arrows indicate NPs contacting the epithelium. Scale bar, 30 μm.

(H) Quantification of individual NP perimeters in contact with the UB epithelium (SD for ctrl 1.08, dko 1.38). ***$p < 0.001$.

(I) Quantification of roundness in NPs contacting the UB epithelium (SD for ctrl 0.03, dko 0.02). *$p < 0.05$.

(J) Polar histogram representing the distribution of angles between NPs and UB epithelium (plot displays 172 ctrl and 150 dko cells; $\overline{x}$ for 70° to 110° ctrl = 63.7, dko = 53.0, and <70° and >110° ctrl = 36.3, dko = 47.0; SD ctrl = 3.2, dko = 4.4). *$p < 0.05$. See also Figure S3. For (H)–(J), n = 3 independent kidneys, each containing 25–65 measurements.

(K and L) Sphere-forming assay performed on dissociated E11.5 NPs with or without FGF2 for 24 hr. Arrows indicate formed spheres. Scale bar, 300 μm.
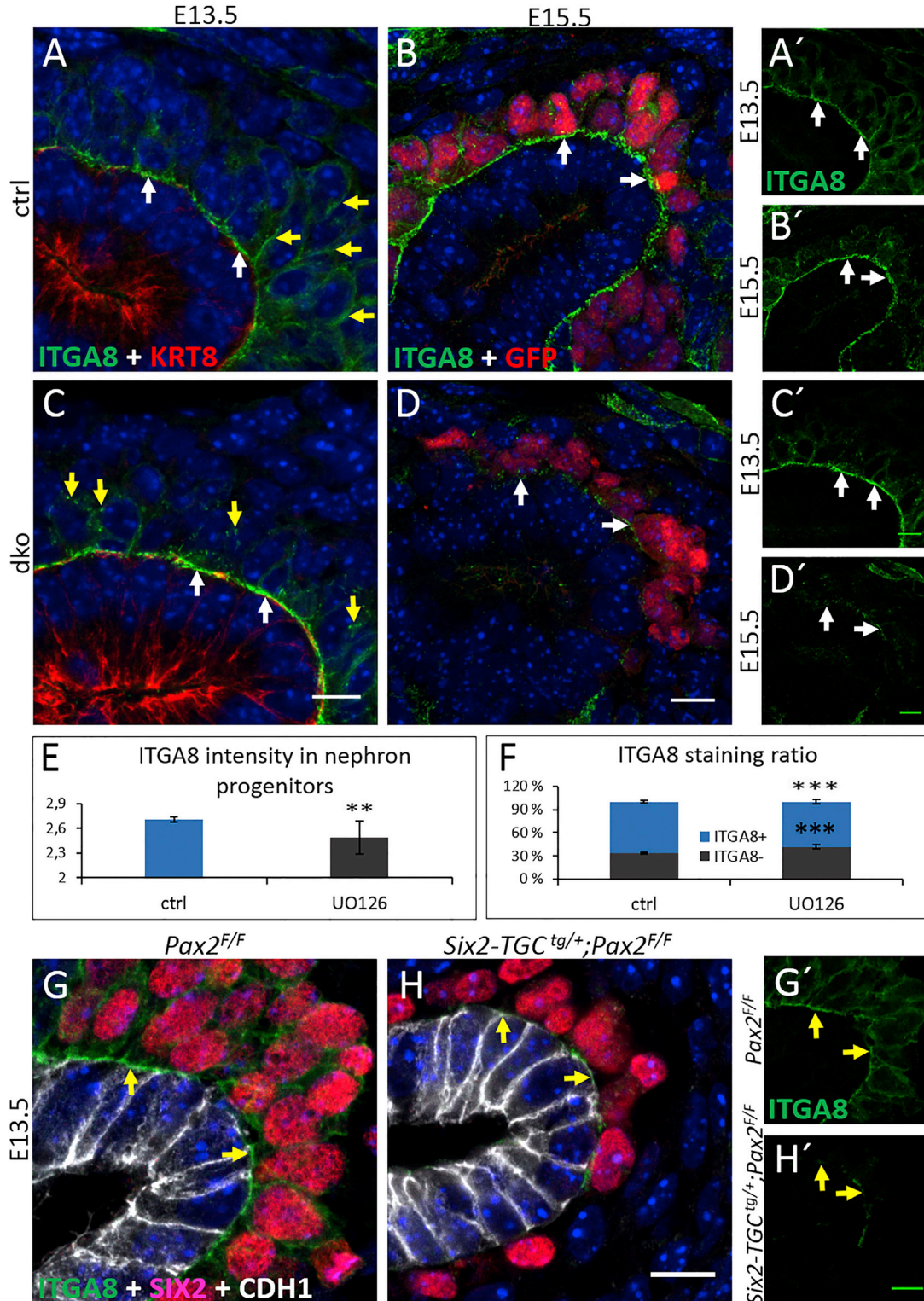
Figure 4. Molecular Regulation of Nephron Progenitor Niche Organization

(A–D) Control (ctrl) and dko embryonic kidneys immunostained for ITGA8 (subset of NP membrane), GFP (*Six2-TGC*[+] NPs), and KRT8 (ureteric bud [UB] epithelium). (A′–D′) Images show only the channel detecting ITGA8. White arrows mark ITGA8 in the basal membranes, and yellow arrows indicate ITGA8 in lateral membranes of NPs in (A) and (C). Scale bars, 10 μm. See also Figures S4 and S5.

(legend continued on next page)

Normal ITGA8 expression in MEK-inhibited embryonic lung lacking PAX2 (Grimley et al., 2017), which we show here to depend on MAPK (Figures 2 and S2), suggests that MAPK activity's regulatory effect on ITGA8 may be subject to NP-specific factors. To test whether the loss of PAX2 impacts ITGA8 expression, we genetically deleted *Pax2* in NPs (*Six2-TGC^{tg/+};Pax2^{F/F}*) and discovered an almost complete loss of ITGA8 by E13.5 (Figures 4G–4H'). Consequently, we propose that MAPK activity sustains NP orientation and niche interactions through PAX2 and ITGA8.

MAPK/ERK Activity Promotes Proliferation in Differentiating Nephrons

NPs differentiate into all segments of the nephron by undergoing typical morphological changes, beginning with the NP condensation into a pretubular aggregate (PA) followed by mesenchymal to epithelial transition to form an epithelial RV. Further morphogenesis depends on proximodistal patterning of the RV that promotes differentiation of nephron segments through comma-shaped bodies (CSBs) and SSBs (O'Brien and McMahon, 2014). Specific localization of MAPK activity to the differentiating nephron precursors (Figures 1D–1I, 1L, S1A–S1C, and S1G) also suggests functions in nephron differentiation. PAs in dko kidneys were morphologically and molecularly comparable with those in control kidneys (Figures 5A, 5B, S2A, S2B, S6A, and S6D). However, UB tips were often associated with either accumulated, undefined PAX2+ mesenchyme or with up to five PAs, whereas only two PAs typically associated with each UB in control kidneys (Figures 5A and 5B). Subsequent quantification of nephron precursor profiles failed to show differences between control and dko kidneys (Figure 5C). However, the number of SSBs showed a 27% decrease in dko kidneys (Figure 5C; p < 0.05), indicating that MAPK activity controls nephron differentiation at a temporally defined stage.

RVs are actively proliferating precursors in which the essential patterning of the prospective nephron is initiated (O'Brien and McMahon, 2014). Strong MAPK activity is seen in the distal RV (Figures 1J and S1G), and quantification of RV sizes showed a 37% drop in dko cell numbers (Figure 5D, p < 0.05). Moreover, distal RVs showed highly reduced cyclin D1 (CCND1) levels in dko kidneys, while a decrease in EdU+ cells was detected specially in proximal RVs (Figures 5E–5H). Thus, MAPK activity regulates proliferation in early nephron precursors similarly as in NPs.

## Nephron Differentiation Requires MAPK/ERK Activity to Propel Proximodistal Patterning

We next studied proximodistal patterning of the RVs and their subsequent epithelialization, manifested by the upregulation of CDH1 and CDH6, cell polarization, and lumen formation. RVs in dko kidneys gained epithelial markers and luminal ZO-1, implying that the change in cellular identity from mesenchymal progenitor to epithelial nephron precursor does not require MAPK activity (Figures 5G, 5H, S6B, S6C, S6E, and S6F). Concurrently to initiation of epithelialization, the RV is subdivided into proximal and distal domains demarcated by spatially restricted protein localizations (O'Brien and McMahon, 2014). LEF1 is first expressed in PA then confined to the distal RV where it indicates active canonical Wnt signaling (Figures 5I and S6A). Notch signaling, activated by the ligand Jagged1 (JAG1), is required for proximal patterning (Figures 5J and 5K) (Cheng et al., 2007). Examination of LEF1 in dko kidneys revealed comparable localization in PAs but a complete absence in distal RVs, while JAG1 generally failed to localize to RVs (Figures 5L–5N and S6D). Subsequently, the transcription factor WT1, which should be upregulated in proximal RV to drive the differentiation of proximal nephron segments (O'Brien and McMahon, 2014), was also missing from dko RVs (Figures 5K and 5N). These data demonstrate that MAPK activity regulates patterning and progression of differentiation in RVs. It also suggests that MAPK activity molecularly primes the RVs to receive and interpret Wnt and Notch pathway signals.

As nephrogenesis progressed to CSB, the absence of distal markers LEF1 and JAG1 persisted in the dko kidneys, and correspondingly WT1 remained unpolarized, while the elongating CSBs maintained CDH1 and CDH6 (Figures 6A–6H, S6G, and S6I). Loss of MAPK activity had no effect on the nephron connection to the UB despite the aberrant precursor morphology and increased apoptosis (Figures 6G, 6H, S6C, and S6F). Of note, dko kidneys, which had significantly fewer SSBs, showed some SSBs comparable with control kidneys (Figures 5C, S6H, and S6J). This is likely due to the failure of a subset of NPs to express CRE (Kobayashi et al., 2008) and suggests that the remaining SSBs in the dko might be descendants of cells with incomplete *Mek1* deletion (Figures S1D–S1F'). Taken together, the MAPK signaling-deficient CSBs are unpatterned and irresponsive to further differentiation signals, leading to nephrogenesis arrest and apoptosis at this stage. A

(E) Flow cytometry analysis of NP population to unstained cell intensity ratio of ITGA8 immunostaining in living cells after 72 hr culture. **p < 0.01.

(F) Flow cytometry analysis of ITGA8+ and ITGA8− cell populations from immunostaining of living cells after 72 hr culture. For (E) and (F), n = 22 ctrl/12 U0126-treated kidney samples each containing 30,000 cells, originating from 15 independent kidneys. ***p < 0.001.

(G and H) Ctrl and *Six2-TGC^{tg/+};Pax2^{F/F}* embryonic kidneys immunostained for ITGA8 (NP membrane), SIX2 (NPs), and CDH1 (UB epithelium). (G' and H') Images show only the channel detecting ITGA8. Arrows mark ITGA8 in the basal membranes of NPs. Scale bars, 10 μm.
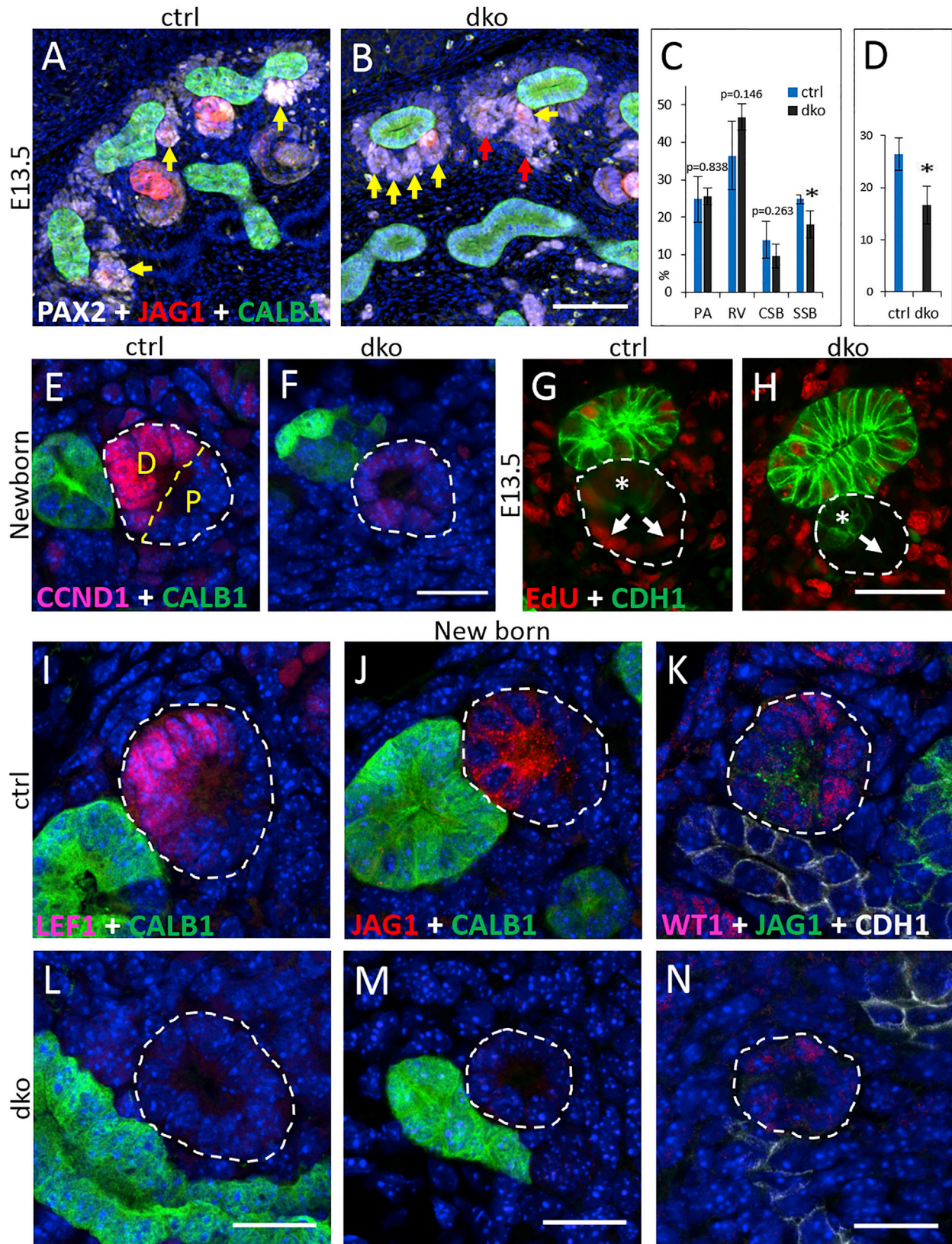
(legend on next page)

comprehensive model of MAPK functions in nephrogenesis is proposed in Figures 6I and 6J.

MAPK/ERK Deficiency Causes Renal Hypodysplasia

Finally, the consequences of disrupted MAPK signaling on the organ level were studied. Kidney size was significantly decreased in the dko pups, while pups retaining one normal *Mek* allele also exhibited a minor change in their kidney size (Figures 7A–7C, S7A, S7D, and S7E; p < 0.001). This difference was not visible at E13.5, but, by E15.5, defects in NP maintenance and nephron differentiation began to impact kidney growth (Figures S7B and S7C). Morphologically, normal newborn (NB) kidneys are divided into the cortex, which is adjacent to the kidney surface and filled with on-going nephrogenesis, and an inner medulla, which is packed with collecting ducts and mature nephron epithelia (Figures 7D and 7E). In addition to severe hypoplasia, dko kidneys exhibited disrupted cortex with mature nephron epithelium and a significantly reduced NP population accompanied by clearly less on-going nephrogenesis (Figures 7F, 2K, and 2N). Also, visualization of nephrons with segment-specific markers revealed a greatly diminished nephron epithelium in the NB dko kidneys (Figures 7G–7J). MEK1 and pERK1/2 staining in NB kidneys showed that all nephrons in dko were formed due to incomplete deletion of *Mek1* by *Six2-TGC*[tg/+], not independently of MAPK activity (Figures S7F–S7I). In summary, disrupting MAPK signaling in NPs results in hypodysplastic kidneys due to a failure to normally expand NPs and advance nephron differentiation, which jointly contribute to premature cessation of nephrogenesis.

DISCUSSION

We examined here the role of MAPK activity in the *in vivo* tissue niche of renal NPs. We found that initially MAPK controls niche organization and NP maintenance, after which it is needed for the progression of differentiation in nephron precursors. Such a dual function of MAPK activity in nephrogenesis aptly adheres to the dynamic changes in its activation and signal transduction strength revealed by live-imaging. The cellular responses to ERK activation depend on the duration and magnitude (Chambard et al., 2007; Pouyssegur et al., 2002), and temporal control is gained by cytosolic phosphatases that rapidly inactivate ERK, producing a transient activation that was observed in the majority of NPs and SSBs. Instead, sustained ERK activation in a subset of NPs and in RVs needs reactivation of a negative feedback loop downstream of ERK activity. Our results suggest that RVs in the developing kidney exploit two different ERK activation mechanisms; MEK-dependent activation drives proliferation in the proximal RV, while sustained ERK activity in the distal domain promotes patterning and differentiation.

Six2CreGFP (*Six2-TGC*[tg/+]) with an incomplete expression pattern in the NPs (Kobayashi et al., 2008; Naiman et al., 2017) was used to abrogate MAPK activity. The limited mature nephron epithelium in the dko kidneys plausibly derives from *Six2-TGC*[tg/+]-negative NPs, which also maintained pERK1/2. Moreover, a recent reports show that *Six2-TGC*[tg/+] transgene itself may cause *Six2* haploinsufficiency (Combes et al., 2018; Volovelsky et al., 2018) and thus interfere with renal differentiation. As originally reported, we also found that *Six2* haploinsufficiency does not affect *Pax2* mRNA or protein, while it significantly impacts CITED1 expression. All our key molecular findings, including altered expression of ITGA8 and PAX2, were generated by comparing control genotypes bearing the *Six2-TGC*[tg/+] transgene with dko, which should minimize the potential effect of *Six2* haploinsufficiency on our findings.

The NP niche is organized around the UB in a highly coherent manner. The individual NPs exhibit columnar alignment and elongated cell shape, which becomes round upon detachment from the UB tips (Combes et al., 2016; Uchiyama et al., 2010). NP cells form contacts

Figure 5. MAPK/ERK-Deficient Nephron Precursors Fail to Proceed through Nephrogenesis

(A and B) Control (ctrl) and dko embryonic kidneys immunostained for PAX2 (NPs, nephron precursors, and UB epithelium), JAG1 (nephron precursors), and CALB1 (UB epithelium). Yellow arrows indicate pretubular aggregates, and red arrows mark undefinable mesenchyme in (B). Scale bar, 100 μm.

(C) Quantification of nephron precursor profiles from paraffin sections, n = 3 independent kidneys, each containing 11–30 measurements. *p < 0.05.
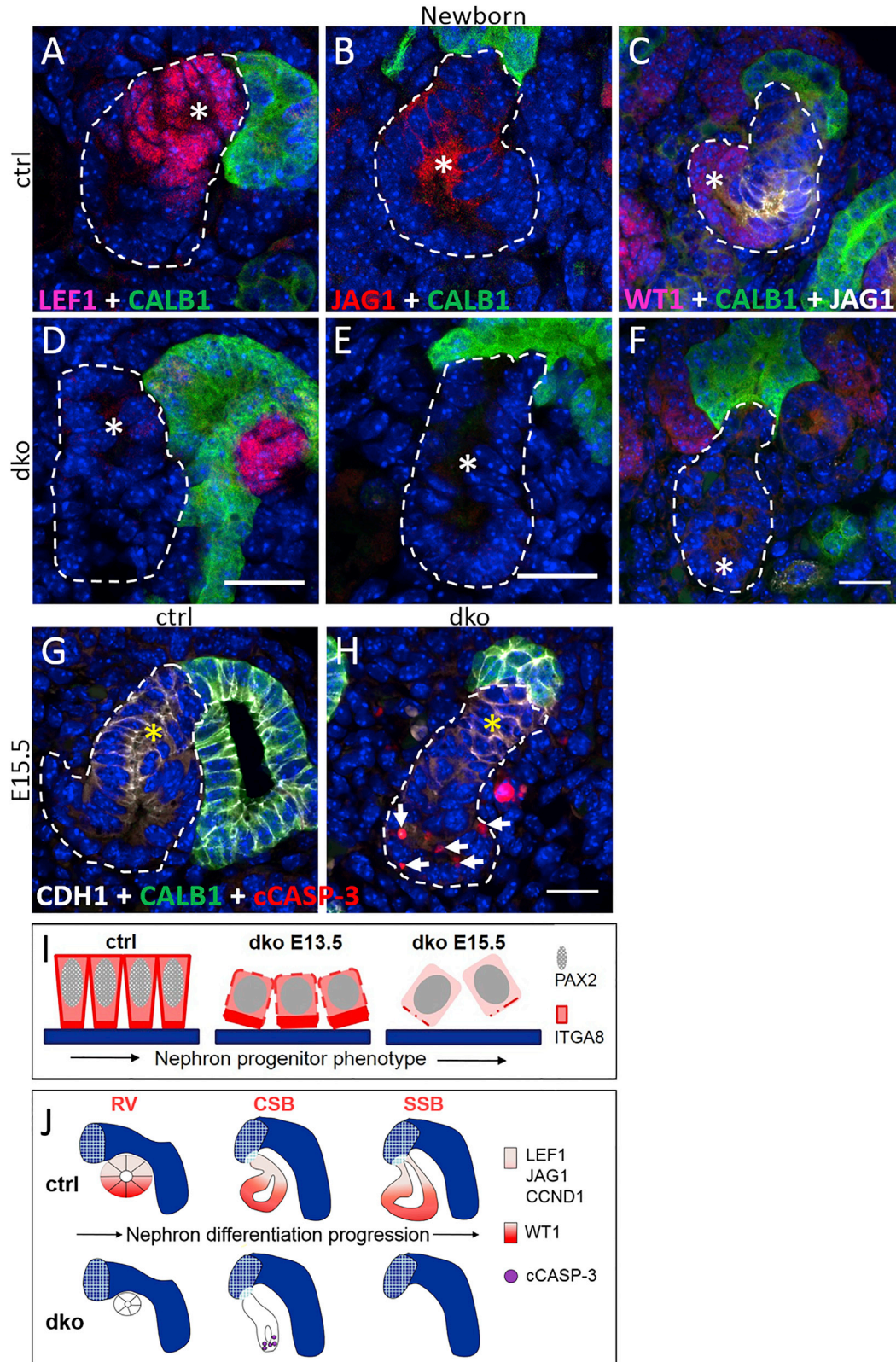
(D) Quantification of renal vesicle (RV) cell amount (n = 3 independent kidneys, each containing 13–18 measurements). *p < 0.05.

For (C) and (D), n = 3 independent kidneys, each containing 11–30 measurements.

(E–H) Ctrl and dko embryonic kidneys immunostained for CCND1 (RV), CDH1 (distal RV and UB epithelium), CALB1, and EdU-labeled (replicating cells). A white dotted line designates the RV. A yellow dotted line separates distal (D) and proximal (P) domains of an RV in (E). Asterisk marks CDH1+ distal RV domain and arrows indicate EdU+ replicative cells in G and H. Scale bars, 20 μm in (F) and 50 μm in (H).

(I–N) Ctrl and dko newborn kidneys immunostained for LEF1, JAG1, WT1 (RV), and CDH1, CALB1. A dotted line designates the RV. Scale bars, 20 μm.

See also Figure S6.

Figure panels A–J

A LEF1 + CALB1 (ctrl)

B JAG1 + CALB1 (ctrl)

C WT1 + CALB1 + JAG1 (ctrl)

D (dko)

E (dko)

F (dko)

G ctrl — E15.5

H dko — E15.5

CDH1 + CALB1 + cCASP-3

I ctrl | dko E13.5 | dko E15.5 — PAX2, ITGA8 — Nephron progenitor phenotype

J RV | CSB | SSB — ctrl / dko — Nephron differentiation progression — LEF1 JAG1 CCND1, WT1, cCASP-3

(legend on next page)

with the UB basement membrane and with neighboring NPs but also with stromal cells, and therefore become exposed to different niche environments and varying intercellular signaling depending on the position of the individual cell. An NP subgroup adjacent to the UB establishes its connection to the epithelium through ITGA8 (Muller et al., 1997). Recent findings suggest that niche-intrinsic, age-dependent changes in the NP population modify surrounding environments and in this way contribute to the control of NP self-renewal (Chen et al., 2015). We found that, in the absence of MAPK activity, PAX2, CITED1, and ITGA8 were disrupted in the NPs. The NP cells lacking MAPK activity also showed changes in cellular properties, which presented with rounder shape, smaller size, and disoriented position, resulting in a gradually increasing overall disorganization within the whole NP niche. After their detachment from the *in vivo* niche, changes in NP cell sizes were no longer detected, perhaps due to the differences in sample population (the first layer *in vivo*, the whole GFP$^+$ population in flow cytometry). The difference may also reflect the actual function of MAPK activity in mediating communication within the NP niche and its surroundings, which is lost when cells are dissociated from each other and their normal environment. All in all, these results suggest that the coherent architecture in renal mesenchyme stems from the highly regulated organization of the UB-adjacent NP population, and identify MAPK activity as an essential molecular regulator mediating those niche-intrinsic changes that have a significant effect on the juxtacrine environment and NP maintenance. Our findings are also in line with results suggesting that niche-intrinsic changes in the NP population can modify the surrounding environment (Chen et al., 2015). In other organ systems, the niche is a critical determinant of biomechanical properties of stem and progenitor cells (Wickstrom and Niessen, 2018).

In addition to extracellular matrix, the NP-intrinsic signals contribute to their maintenance and creation of the niche environment (O'Brien and McMahon, 2014). We found that MAPK activity is selectively required for the expression of certain NP regulators, namely PAX2 and CITED1, without affecting others, such as SIX2 and WT1, all known to control NP viability, self-renewal, and identity (Boyle et al., 2007; Naiman et al., 2017; Park et al., 2012). Previous studies show that disruption of PAX2 function leads to a rapid loss of NPs, with round cell morphology and dispersion of the NPs into the surrounding stroma (Grimley et al., 2017; Naiman et al., 2017; Rothenpieler and Dressler, 1993), a phenotype very reminiscent of MAPK deficiency. Regulation of PAX2 by MAPK signaling is not observed in cell culture where PAX2 phosphorylation generally increases its transactivation potential (Cai et al., 2002), whereas interactions with the co-repressor TLE4 inhibits phosphorylation of PAX2 (Cai et al., 2003). MAPK phosphorylation of TLE weakens its repressor activity, thus providing a prospective mechanism by which MAPK may regulate PAX2 (Hasson et al., 2005). Interestingly, CITED1, which is proposed to demarcate the uninduced NP population among all NP cells, is a direct target of PAX2 (Brown et al., 2013). As loss of *Cited1*, even in combination with *Cited2*, has no impact on kidney development (Boyle et al., 2007), it is likely that the dearth of CITED1 in dko kidneys merely reflects the reduced PAX2 levels.

Consistently with our findings, FGF-activated FGFR1/2 signaling is crucial for the maintenance of NPs and *Pax2* expression in this population (Barak et al., 2012; Poladia et al., 2006). Genetic loss of ligands FGF9/20 results in premature NP differentiation (Barak et al., 2012), which is different from our findings in MAPK-deficient kidneys, where NPs are exhausted due to maintenance failure, but differentiation is relatively normal up to the RV patterning and expansion. Somewhat similarly to our results, *in vitro* NP cell cultures supplemented with FGF9 showed improved survival and proliferation, supporting the idea that FGF signaling would also regulate NP cell maintenance (Brown et al., 2015). Moreover, the *Fgf8* expression domain overlaps with MAPK activity in RVs, and disruption of FGF8 function results in nephrogenesis phenotypes similar to those in MAPK dko kidneys (Grieshammer et al., 2005; Perantoni et al., 2005). Taken together, these results suggest that FGF signaling is the likely major upstream RTK that

Figure 6. MAPK/ERK-Deficient Nephron Precursors Are Apoptotic and Arrest Nephrogenesis Prematurely
(A–H) Control (ctrl) and dko embryonic kidneys immunostained for LEF1, JAG1, WT1 (CSB), cCASP-3 (apoptotic cells), CDH1 (CSB and ureteric bud [UB] epithelium), and CALB1 (UB epithelium). A dotted line designates the CSB. Asterisks mark LEF1$^+$, JAG1$^+$, and WT1$^+$ domains in (A)–(F), and show the CDH1$^+$ distal domain in (G) and (H). Arrows indicate cCASP-3$^+$ apoptotic cells in (H). Scale bars, 20 μm.
(I) Schematic summary of the NP phenotype in ctrl and dko embryonic kidneys. The pink columns represent the NP cells, and the horizontal blue bar represents UB epithelium. Red illustrates ITGA8 expression and gray/white shows nuclear PAX2, which is reduced (gray) in dko NPs.
(J) Schematic summary of nephron differentiation in ctrl and dko embryonic kidneys. The red and pale pink circles, adjacent to the blue UB epithelium, represent the patterned renal vesicle (RV) as it proceeds through CSB to SSB stage. LEF1, JAG1, and CCND1 localize in the pale pink regions of the differentiating nephrons, while WT1 is found in the red segment. Lilac dots represent cCASP-3$^+$ apoptotic cells.
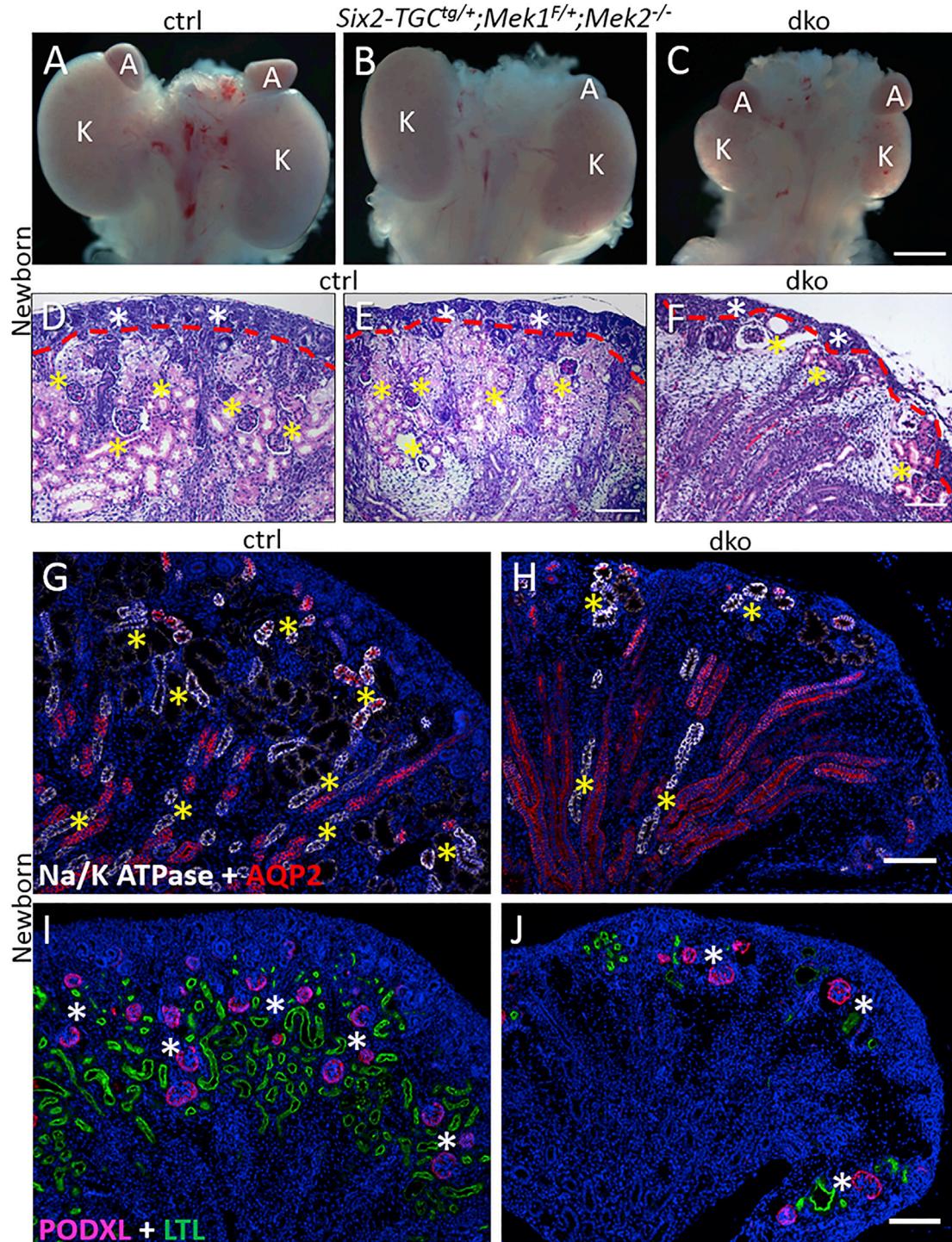See also Figure S6.

Figure 7. MAPK/ERK Depletion from NPs Leads to Hypodysplastic Kidneys with Reduced Nephrons

(A–C) Whole-mount view of control (ctrl), *Six2-TGC^{tg/+};Mek1^{F/+};Mek2^{−/−}*, and dko newborn kidneys (K, kidney; A, adrenal gland). Scale bar, 1 mm.

(D–F) Histology in ctrl and dko newborn kidneys. A dotted line indicates the boundary between kidney cortex (white asterisks) and medulla. Yellow asterisks show glomeruli and mature nephron epithelia. Scale bars, 100 μm.

(legend continued on next page)

is activating the MAPK pathway in nephrogenesis. The data also provide evidence that NP properties and niche organization in the developing kidney are controlled by MAPK activity, which similarly to FGF signaling, is required for normal expression of PAX2.

Active canonical Wnt signaling, indicated by the expression of LEF1 together with CCND1, is essential for specification and patterning of the nephron (Lindstrom et al., 2015; O'Brien and McMahon, 2014). Furthermore, MAPK signaling is known to initiate expression of the Notch ligand JAG1 in many cell types (Saravanamuthu et al., 2009). Notch signaling has a prominent function in defining the proximal domains of differentiating nephrons as shown in Notch signaling-deficient kidneys, where precursors fail to differentiate into SSBs. In addition, WT1 has been indicated in driving proximal differentiation and regulation of gene expression mediated by Notch signaling (O'Brien and McMahon, 2014). Our study demonstrates that the MAPK pathway is dispensable for PA formation but is critically important for further nephron differentiation. Peculiarly, we occasionally observed an accumulation of undefined PAX2^{+} nephrogenic mass under the T-shaped UB in dko kidneys, but causes and consequences of this remain to be elucidated. We demonstrate that MAPK activity is needed in RVs to distally express LEF1, CCND1, and JAG1, as well as to proximally upregulate WT1. Thus, based on our results, we propose that the MAPK pathway plays a dual function in nephrogenesis; it is essential for PAX2 and ITGA8 expression as well as coherence and maintenance of NPs, and it primes RV cells to become receptive for subsequent nephron differentiation, which is triggered by canonical Wnt and Notch signaling.

EXPERIMENTAL PROCEDURES

Mouse Lines

Details of mouse lines used are provided in Supplemental Information. Animal husbandry and procedures were approved by EU legislation and the Finnish Animal Care and Use Committee, by the Animal Care and Use Committee of Kyoto University Graduate School of Medicine (no.10584), and by the University Committee on Use and Care of Animals at the University of Michigan.

Immunostaining, H&E Staining, EdU Labeling, and Imaging

Tissue processing, immunostaining H&E staining, and EdU labeling were performed as described previously (Ihermann-Hella et al., 2014). See Supplemental Information for experiment specifications and imaging information.

Data Quantification and Statistical Analyses

Quantification of data was performed with the Fiji ImageJ program (Schindelin et al., 2012), if not stated otherwise, and represented as average values ± SD. Details of data quantification are provided in Supplemental Information. Significance was tested with independent-samples two-tailed t test employing SPSS Statistics software (IBM) or t test with pooled SD comparisons (p value adjustment with Holm method) using R (R Core Team, 2013). Pearson correlation coefficient was used for correlation calculation.

Measurement of Cellular Properties

Quantification of NP perimeter, roundness, contact surface length, and angle toward UB epithelium was obtained from paraffin sections stained with CTNND1, CALB1, and Hoechst. See Supplemental Information for details.

Cell-Cycle Analysis

$Six2$-$TGC^{tg/+}$-containing control (n = 34) and dko (n = 22) E13.5 kidneys were dissociated into single-cell suspensions with 0.25% trypsin, and GFP^{+} NP cells were isolated using fluorescence-activated cell sorting (FACS) with a Sony SH800Z cell sorter. Cells were subsequently fixed with 70% EtOH, treated with RNAse A (Thermo Fisher Scientific), and stained with propidium iodide (Invitrogen). DNA content-based cell-cycle analysis was performed with an Accuri C6 flow cytometer (BD Biosciences) and FlowJo software (BD Biosciences). For a total of 10,000 NP cells per genotype, four distinct ctrl and dko kidneys were used, and this was independently repeated three to four times. See Supplemental Information for ITGA8 analysis in live cells and additional flow cytometry analyses.

Tissue Culture and Live Imaging of FRET Biosensor-Expressing Kidneys

Dissected E12.5 kidneys and lungs were placed on Transwell polyester membrane supports (Corning) and cultured at the air-liquid interface at 37°C, under 5% CO_2. For live imaging, a 35-mm glass-based dish (Iwaki) and culture with FluoroBrite DMEM (Thermo Fischer Scientific) were used. See Supplemental Information for details.

Sphere-Forming Assay

Metanephric mesenchymes from E11.5 NMRI kidneys were dissociated into single-cell suspension with TrypLE Express (Gibco), plated on 3D Matrigel in a chamber slide system (Lab-Tek), and cultured under kidney culture conditions for 24 hr, supplemented with 10 μM PP2 (Calibochem). MAPK activation was performed with 50 ng/mL FGF2 (Peprotech). Images were acquired with Zeiss

---

(G–J) Ctrl and dko newborn kidneys immunostained for Na/K ATPase (ascending limb of loop of Henle), AQP2 (collecting ducts), PODXL (glomeruli), and LTL (proximal tubules). Asterisks indicate Na/K ATPase[+] mature distal nephron epithelia in (G) and (H), and glomeruli and mature proximal nephron epithelia in (I) and (J). Scale bars, 100 μm.
See also Figure S6.

Axiovert 25, and time-lapse imaging was performed with Nikon Eclipse Ti-E microscope. Experiments were repeated three times, pooling 8–14 mesenchymes to one sample.

Transmission Electron Microscopy

Sample preparation from E13.5 kidneys and imaging were described earlier (Ihermann-Hella et al., 2014). One kidney from each genotype was sectioned and imaged from four representative levels.

Cell Culture and Western Blot Analysis

The assay was performed with mK4 cells followed by western blotting and analysis with standard methods (see Supplemental Information for details). The data were collected from four independent experiments.

SUPPLEMENTAL INFORMATION

Supplemental Information includes Supplemental Experimental Procedures, seven figures, one table, and four videos and can be found with this article online at https://doi.org/10.1016/j.stemcr.2018.08.012.

AUTHOR CONTRIBUTIONS

A.I.-H., J.K., and K.K. performed the majority of dko characterization-related experiments. T.H. and M.M. did the FRET imaging and quantification. I.M. is responsible for electron microscopy. A.D. conducted the sphere assays. H.L. and H.N.K. analyzed PAX2 levels in cell cultures. C.C., A.S., and G.R.D. provided *Pax2*$^{F/F}$ and *Six2-TGC*$^{tg/+}$;*Pax2*$^{F/F}$ kidney sections. A.I.-H. and T.H. prepared the figures. A.I.-H. together with S.K. planned the experiments, analyzed the results, and wrote the manuscript.

REFERENCES

Barak, H., Huh, S.H., Chen, S., Jeanpierre, C., Martinovic, J., Parisot, M., Bole-Feysot, C., Nitschke, P., Salomon, R., Antignac, C.,

et al. (2012). FGF9 and FGF20 maintain the stemness of nephron progenitors in mice and man. Dev. Cell *22*, 1191–1207.

Boucherat, O., Nadeau, V., Berube-Simard, F.A., Charron, J., and Jeannotte, L. (2015). Crucial requirement of ERK/MAPK signaling in respiratory tract development. Development *142*, 3801.

Boyle, S., Shioda, T., Perantoni, A.O., and de Caestecker, M. (2007). Cited1 and Cited2 are differentially expressed in the developing kidney but are not required for nephrogenesis. Dev. Dyn. *236*, 2321–2330.

Brown, A.C., Adams, D., de Caestecker, M., Yang, X., Friesel, R., and Oxburgh, L. (2011). FGF/EGF signaling regulates the renewal of early nephron progenitors during embryonic development. Development *138*, 5099–5112.

Brown, A.C., Muthukrishnan, S.D., Guay, J.A., Adams, D.C., Schafer, D.A., Fetting, J.L., and Oxburgh, L. (2013). Role for compartmentalization in nephron progenitor differentiation. Proc. Natl. Acad. Sci. USA *110*, 4640–4645.

Brown, A.C., Muthukrishnan, S.D., and Oxburgh, L. (2015). A synthetic niche for nephron progenitor cells. Dev. Cell *34*, 229–241.

Cai, Y., Lechner, M.S., Nihalani, D., Prindle, M.J., Holzman, L.B., and Dressler, G.R. (2002). Phosphorylation of Pax2 by the c-Jun N-terminal kinase and enhanced Pax2-dependent transcription activation. J. Biol. Chem. *277*, 1217–1222.

Cai, Y., Brophy, P.D., Levitan, I., Stifani, S., and Dressler, G.R. (2003). Groucho suppresses Pax2 transactivation by inhibition of JNK-mediated phosphorylation. EMBO J. *22*, 5522–5529.

Chambard, J.C., Lefloch, R., Pouyssegur, J., and Lenormand, P. (2007). ERK implication in cell cycle regulation. Biochim. Biophys. Acta *1773*, 1299–1310.

Chen, S., Brunskill, E.W., Potter, S.S., Dexheimer, P.J., Salomonis, N., Aronow, B.J., Hong, C.I., Zhang, T., and Kopan, R. (2015). Intrinsic age-dependent changes and cell-cell contacts regulate nephron progenitor lifespan. Dev. Cell *35*, 49–62.

Cheng, H.T., Kim, M., Valerius, M.T., Surendran, K., Schuster-Gossler, K., Gossler, A., McMahon, A.P., and Kopan, R. (2007). Notch2, but not Notch1, is required for proximal fate acquisition in the mammalian nephron. Development *134*, 801–811.

Combes, A.N., Lefevre, J.G., Wilson, S., Hamilton, N.A., and Little, M.H. (2016). Cap mesenchyme cell swarming during kidney development is influenced by attraction, repulsion, and adhesion to the ureteric tip. Dev. Biol. *418*, 297–306.

Combes, A.N., Wilson, S., Phipson, B., Binnie, B.B., Ju, A., Lawlor, K.T., Cebrian, C., Walton, S.L., Smyth, I.M., Moritz, K.M., et al. (2018). Haploinsufficiency for the Six2 gene increases nephron progenitor proliferation promoting branching and nephron number. Kidney Int. *93*, 589–598.

Corson, L.B., Yamanaka, Y., Lai, K.M., and Rossant, J. (2003). Spatial and temporal patterns of ERK signaling during mouse embryogenesis. Development *130*, 4527–4537.

Donovan, M.J., Natoli, T.A., Sainio, K., Amstutz, A., Jaenisch, R., Sariola, H., and Kreidberg, J.A. (1999). Initial differentiation of the metanephric mesenchyme is independent of WT1 and the ureteric bud. Dev. Genet. *24*, 252–262.

Grieshammer, U., Cebrian, C., Ilagan, R., Meyers, E., Herzlinger, D., and Martin, G.R. (2005). FGF8 is required for cell survival at

distinct stages of nephrogenesis and for regulation of gene expression in nascent nephrons. Development *132*, 3847–3857.

Grimley, E., Liao, C., Ranghini, E.J., Nikolovska-Coleska, Z., and Dressler, G.R. (2017). Inhibition of Pax2 transcription activation with a small molecule that targets the DNA binding domain. ACS Chem. Biol. *12*, 724–734.

Hartman, H.A., Lai, H.L., and Patterson, L.T. (2007). Cessation of renal morphogenesis in mice. Dev. Biol. *310*, 379–387.

Hasson, P., Egoz, N., Winkler, C., Volohonsky, G., Jia, S., Dinur, T., Volk, T., Courey, A.J., and Paroush, Z. (2005). EGFR signaling attenuates Groucho-dependent repression to antagonize Notch transcriptional output. Nat. Genet. *37*, 101–105.

Ihermann-Hella, A., Lume, M., Miinalainen, I.J., Pirttiniemi, A., Gui, Y., Peranen, J., Charron, J., Saarma, M., Costantini, F., and Kuure, S. (2014). Mitogen-activated protein kinase (MAPK) pathway regulates branching by remodeling epithelial cell adhesion. PLoS Genet. *10*, e1004193.

Kobayashi, A., Valerius, M.T., Mugford, J.W., Carroll, T.J., Self, M., Oliver, G., and McMahon, A.P. (2008). Six2 defines and regulates a multipotent self-renewing nephron progenitor population throughout mammalian kidney development. Cell Stem Cell *3*, 169–181.

Komatsu, N., Aoki, K., Yamada, M., Yukinaga, H., Fujita, Y., Kamioka, Y., and Matsuda, M. (2011). Development of an optimized backbone of FRET biosensors for kinases and GTPases. Mol. Biol. Cell *22*, 4647–4656.

Lindstrom, N.O., Carragher, N.O., and Hohenstein, P. (2015). The PI3K pathway balances self-renewal and differentiation of nephron progenitor cells through beta-catenin signaling. Stem Cell Reports *4*, 551–560.

Little, M.H. (2016). Growing kidney tissue from stem cells: how far from "party trick" to medical application? Cell Stem Cell *18*, 695–698.

McKay, M.M., and Morrison, D.K. (2007). Integrating signals from RTKs to ERK/MAPK. Oncogene *26*, 3113–3121.

Muller, U., Wang, D., Denda, S., Meneses, J.J., Pedersen, R.A., and Reichardt, L.F. (1997). Integrin alpha8beta1 is critically important for epithelial-mesenchymal interactions during kidney morphogenesis. Cell *88*, 603–613.

Naiman, N., Fujioka, K., Fujino, M., Valerius, M.T., Potter, S.S., McMahon, A.P., and Kobayashi, A. (2017). Repression of interstitial identity in nephron progenitor cells by Pax2 establishes the nephron-interstitium boundary during kidney development. Dev. Cell *41*, 349–365.e3.

Narva, E., Stubb, A., Guzman, C., Blomqvist, M., Balboa, D., Lerche, M., Saari, M., Otonkoski, T., and Ivaska, J. (2017). A strong contractile actin fence and large adhesions direct human pluripotent colony morphology and adhesion. Stem Cell Reports *9*, 67–76.

O'Brien, L.L., and McMahon, A.P. (2014). Induction and patterning of the metanephric nephron. Semin. Cell Dev. Biol. *36*, 31–38.

Parada, C., Han, D., Grimaldi, A., Sarrion, P., Park, S.S., Pelikan, R., Sanchez-Lara, P.A., and Chai, Y. (2015). Disruption of the ERK/MAPK pathway in neural crest cells as a potential cause of Pierre Robin sequence. Development *142*, 3734–3745.

Park, J.S., Ma, W., O'Brien, L.L., Chung, E., Guo, J.J., Cheng, J.G., Valerius, M.T., McMahon, J.A., Wong, W.H., and McMahon, A.P. (2012). Six2 and Wnt regulate self-renewal and commitment of nephron progenitors through shared gene regulatory networks. Dev. Cell *23*, 637–651.

Perantoni, A.O., Timofeeva, O., Naillat, F., Richman, C., Pajni-Underwood, S., Wilson, C., Vainio, S., Dove, L.F., and Lewandoski, M. (2005). Inactivation of FGF8 in early mesoderm reveals an essential role in kidney development. Development *132*, 3859–3871.

Poladia, D.P., Kish, K., Kutay, B., Hains, D., Kegg, H., Zhao, H., and Bates, C.M. (2006). Role of fibroblast growth factor receptors 1 and 2 in the metanephric mesenchyme. Dev. Biol. *291*, 325–339.

Pouyssegur, J., Volmat, V., and Lenormand, P. (2002). Fidelity and spatio-temporal control in MAP kinase (ERKs) signalling. Biochem. Pharmacol. *64*, 755–763.

R Core Team (2013). R: A Language and Environment for Statistical Computing (R Foundation for Statistical Computing).

Roskoski, R., Jr. (2012). ERK1/2 MAP kinases: structure, function, and regulation. Pharmacol. Res. *66*, 105–143.

Rothenpieler, U.W., and Dressler, G.R. (1993). Pax-2 is required for mesenchyme-to-epithelium conversion during kidney development. Development *119*, 711–720.

Saravanamuthu, S.S., Gao, C.Y., and Zelenka, P.S. (2009). Notch signaling is required for lateral induction of Jagged1 during FGF-induced lens fiber differentiation. Dev. Biol. *332*, 166–176.

Schindelin, J., Arganda-Carreras, I., Frise, E., Kaynig, V., Longair, M., Pietzsch, T., Preibisch, S., Rueden, C., Saalfeld, S., Schmid, B., et al. (2012). Fiji: an open-source platform for biological-image analysis. Nat. Methods *9*, 676–682.

Scholl, F.A., Dumesic, P.A., Barragan, D.I., Harada, K., Bissonauth, V., Charron, J., and Khavari, P.A. (2007). Mek1/2 MAPK kinases are essential for mammalian development, homeostasis, and Raf-induced hyperplasia. Dev. Cell *12*, 615–629.

Self, M., Lagutin, O.V., Bowling, B., Hendrix, J., Cai, Y., Dressler, G.R., and Oliver, G. (2006). Six2 is required for suppression of nephrogenesis and progenitor renewal in the developing kidney. EMBO J. *25*, 5214–5228.

Short, K.M., Combes, A.N., Lefevre, J., Ju, A.L., Georgas, K.M., Lamberton, T., Cairncross, O., Rumballe, B.A., McMahon, A.P., Hamilton, N.A., et al. (2014). Global quantification of tissue dynamics in the developing mouse kidney. Dev. Cell *29*, 188–202.

Uchiyama, Y., Sakaguchi, M., Terabayashi, T., Inenaga, T., Inoue, S., Kobayashi, C., Oshima, N., Kiyonari, H., Nakagata, N., Sato, Y., et al. (2010). Kif26b, a kinesin family gene, regulates adhesion of the embryonic kidney mesenchyme. Proc. Natl. Acad. Sci. USA *107*, 9240–9245.

Volovelsky, O., Nguyen, T., Jarmas, A.E., Combes, A.N., Wilson, S.B., Little, M.H., Witte, D.P., Brunskill, E.W., and Kopan, R. (2018). Hamartin regulates cessation of mouse nephrogenesis independently of Mtor. Proc. Natl. Acad. Sci. USA *115*, 5998–6003.

Wickstrom, S.A., and Niessen, C.M. (2018). Cell adhesion and mechanics as drivers of tissue organization and differentiation: local cues for large scale organization. Curr. Opin. Cell Biol. *54*, 89–97.